FULL PAPER

DOI: 10.1002/chem.200((……))

Metal Ion-Dependent Biological Properties of a Chelator-Derivatised Somatostatin Analogue for Tumour Targeting

Axel Heppeler[a]+, João P. André[b]+, Ingeborg Buschmann[a], Xuejuan Wang[a], Jean-Claude Reubi[c], Michael Hennig[d], Thomas A. Kaden[e], Helmut R. Maecke*[a]

Abstract: Somatostatin-based radioligands were shown to have sensitive imaging properties for neuroendocrine tumours and their metastases. The potential of [^{55}Co]DOTATOC (DOTATOC = 4,7, 10-tricarboxymethyl-1,4,7,10-tetraazacyclododecane-1-yl-acetyl-D-Phe-Lys-Tyr-D-Trp-Lys-Thr-Lys-1-threoninol (disulfide bond) as a new radiopharmaceutical agent for PET was evaluated. ^{57}Co was used as a surrogate of the positron emitter ^{55}Co and the pharmacokinetics of [^{57}Co]DOTATOC was investigated using two nude mouse models. The somatostatin receptor subtype (sst1-5) affinity profile of [^{nat}Co]DOTA-TOC was assessed using autoradiographic methods on membranes transfected with human somatostatin receptor subtypes. These studies revealed that [^{57}Co]DOTATOC is an sst2-specific radiopeptide presenting the highest affinity ever found for the sst2 receptor subtype.
The rate of internalisation into the AR4-2J cell line also was the highest found for any somatostatin-based radiopeptide.
Biodistribution studies, performed in nude mice bearing the AR4-2J tumour or a transfected HEK-sst2 cell-based tumour, showed high and specific uptake in the tumour and in other sst receptor-expressing tissues reflecting the high receptor binding affinity and the high rate of internalisation.
The pharmacologic differences between [^{57}Co]DOTATOC and [^{67}Ga]DOTA-TOC were discussed in terms of the structural parameters found for the chelate models $Co^{II}(DOTA)^{2-}$ and $Ga^{III}(DOTA)^{-}$, whose X-ray structures were determined. Both chelates show sixfold coordination in pseudooctahedral arrangements.

Keywords: antitumour agents · radiocobalt · somatostatin · PET · radiopharmaceuticals

Introduction

The use of radionuclides in medical fields such as molecular imaging and targeted radionuclide therapy is in rapid expansion[1, 2]. Radiolabeled bioactive peptides are currently being employed in tumour targeting using both Positron Emission Tomography (PET) and Single Photon Emission Computed Tomography (SPECT)[3-9]. PET is an imaging modality with the advantage of high spatial resolution, high sensitivity, and the potential of quantification. For these reasons it is nowadays considered one of the most powerful tools for molecular imaging. Bioactive peptides labelled with metallic particle-emitting isotopes, such as $^{90}Y^{III}$ or $^{177}Lu^{III}$, allow peptide receptor-mediated radionuclide therapy (PRMRT)[10].

The first regulatory peptides developed for radiopharmaceutical applications have been somatostatin analogues, which are being employed in the diagnosis of somatostatin receptor-positive tumours when modified with the chelator DTPA (diethylenetriaminepentaacetic acid) and labelled with the γ-emitter ^{111}In[11].

Somatostatin is a tetradecapeptide produced by neuroendocrine, inflammatory and immune cells and is thought to be an important physiological regulator of numerous functions. Its action is mediated by five receptor subtypes (sst1-sst5), which belong to the G-protein coupled receptor family. All subtype receptors have been found to be overexpressed to some degree in different tumours, often concomitantly on the same cell[12]. By far most important is the overexpression of receptor subtype 2. It is therefore

[a] Dr. Axel Heppeler, Dr. Xuejuan Wang, Prof. Helmut R. Maecke
Division of Radiological Chemistry
University Hospital of Basel
CH-4031 Basel, Switzerland
Fax: (+)41 61 265 4699
E-mail: hmaecke@uhbs.ch
[b] Prof. João P. André
Centro de Química
Campus de Gualtar
Universidade do Minho
4710-057 Braga, Portugal
[c] Prof. Jean Claude Reubi
Division of Cell Biology and Experimental Cancer Research
Institute of Pathology
University of Berne
Murtenstrasse 31
CH-3010 Berne, Switzerland
[d] Dr. Michael Hennig
Hoffman-La Roche Ltd
Pharma Research, X-ray Crystallography
CH-4070 Basel, Switzerland
[e] Prof. Thomas A. Kaden, Dr. Ingeborg Buschmann
Institute of Inorganic Chemistry
University of Basel
Spitalstrasse 51
CH-4056 Basel, Switzerland
+ These two authors contributed equally to the manuscript

Supporting information for this article is available on the WWW under

conceivable to search for somatostatin analogues with improved affinity to sst2.

We have developed a DOTA (DOTA = 1,4,7,10-tetraazacyclododecane-N,N´,N´´,N´´´-tetraacetic acid)-derivatised somatostatin analogue, [DOTA^0,Tyr^3]-octreotide (DOTATOC, Figure 1),[13] which has been successfully labelled with radiometals and proven to be useful in different areas of diagnostic and therapeutic nuclear oncology[14]. In particular the $^{68}Ga^{III}$-labelled peptide is currently being used in several European centres, affording very sensitive images of a variety of human tumours and showing an improved diagnostic accuracy, superior to other radiological imaging modalities such as [^{111}In]DOTATOC[15]. The ^{68}Ga-DOTATOC shows approximately 5-fold higher binding affinity to sst2 than [^{111}In/^{90}Y]DOTATOC ; in addition, it shows a higher rate of internalisation into sst2-expressing tumour cells, an approximately 2.5-fold higher tumour uptake and a significantly lower kidney uptake in animals and patients. We have previously shown that this difference in the biological behaviour of metallopeptides may be attributed to structural differences within the chelate moiety[13, 16].

((Insert Figure 1 here))

Figure 1. Structural formulae of [DOTA^0,Tyr^3]-octreotide (DOTATOC) (above) and. DOTA-D-PheNH$_2$ (below).

A crystallographic study of the Ga^{III}- and Y^{III}-chelates of the model peptide DOTA-D-PheNH$_2$ (Figure 1) showed differences in their geometry. Ga^{III}(DOTA-D-PheNH$_2$) is hexacoordinated with pseudooctahedral *cis*-geometry and a folded macrocyclic unit whereas the structure of Y^{III}(DOTA-D-PheNH$_2$) has eight-fold coordination including the amide carboxy oxygen with a somewhat distorted square-antiprismatic geometry. Distant from the pharmacophore of the molecule, this structural difference within the metal chelate leads to a five times higher receptor affinity and probably is also responsible for the mentioned improved biodistribution of the radiogallium-labelled compound. This superiority could also be confirmed clinically using [^{68}Ga]DOTATOC in PET[17] and [^{67}Ga]DOTATOC in SPECT[13, 18]. This finding prompted us to exploit such structural features when using another positron-emitting metal, namely $^{55}Co^{II}$ ($t_{1/2}$ 17.5 h, β^+ (77%), EC (23%)). While the structures of the Ga^{III}- and Co^{II}-labelled peptides are expected to be similar, the use of the longer-lived cyclotron-produced $^{55}Co^{II}$ as PET radiometal could allow imaging at later time points when target-to-background ratios are higher. In the literature there are reports of the use of $^{55}Co^{II}$ as a PET radiometal in medical fields that range from cerebrovascular diseases[19-21] to studies of human lymphocyte distribution[22] and [^{55}Co]EDTA-based quantitative imaging of the kidneys[23].

In the present work we used $^{57}Co^{II}$ ($t_{1/2}$ 270 d, E_γ = 122 keV (86%), 136 keV (10%)) as a surrogate of $^{55}Co^{II}$ to study the biodistribution of [^{57}Co]DOTATOC in two mouse tumour models and also to compare its receptor binding affinity and subtype specificity with those of [$^{67/68}$Ga]DOTATOC and [^{90}Y]DOTATOC. In addition, X-ray studies of Co^{II}(DOTA)$^{2-}$ and Ga^{III}(DOTA)$^-$, two model chelates with relevance to the monoamide structures of the peptide derivatives, were performed with the aim of potentially understanding the differences and similarities in the biological behaviour of the different radiometal-labelled peptides.

Results and Discussion

Synthesis, labelling and stability: The preparation of DOTATOC involves the coupling of the monoreactive DOTA(tBu)$_3$-prochelator to the solid phase-assembled, side chain-protected peptide, as described in Ginj et al[24]. The model DOTA-peptide, DOTA-D-PheNH$_2$, was synthesised in a similar way. DOTATOC was labelled with $^{57}Co^{II}$ in acetate buffer (pH 5) by heating (95°C, 30 min); the labelling yield was >99.5% at a specific activity of 5 mCi/µmol. Co^{II}(DOTA-D-PheNH$_2$)$^-$, Co^{II}(DOTA)$^{2-}$ and Ga^{III}(DOTA)$^-$ were prepared by adding the ligand and metal chloride or nitrate in water and heating (95°C, 30 min). Slow evaporation of aqueous solutions of Co^{II}(DOTA)$^{2-}$ and Ga^{III}(DOTA)$^-$ afforded single crystals suitable for X-ray analysis.

To understand the pharmacologic differences between [^{67}Ga]DOTATOC and [^{57}Co]DOTATOC we set out NMR-experiments to establish the oxidation state of cobalt in the model chelates and in [^{57}Co]DOTATOC. Labelling and complexation reactions were performed at elevated temperatures and in aerated solution which may cause autoxidation of Co^{II}. Cobalt occurs naturally as the mononuclear isotope ^{59}Co, which has a nuclear spin I=7/2, a relative large nuclear quadrupole moment and its chemical shifts in different chemical environments span a range of 18000 ppm. Contrary to Co^{III} the Co^{II} ion (d^7) is paramagnetic and its complexes are therefore beyond the scope of ^{59}Co NMR investigation.

We performed ^{59}Co NMR spectroscopy with the model chelate Co^{II}(DOTA-D-PheNH$_2$) and established the absence of ^{59}Co NMR signal in a wide spectral window in aqueous solution. This is consistent with a +2 oxidation state. In an octahedral environment, divalent cobalt may be found in two different electronic states: a low spin $t_{2g}^6e_g^1$ state with one unpaired electron (S=1/2) and a high spin state $t_{2g}^5e_g^2$ with three unpaired electrons (S=3/2). The colour of the chelate is consistent with a high spin octahedral species, typically pale red or purple. Another strong indication for the high spin assignment comes from the X-ray structure. Low spin octahedral Co^{II} complexes undergo Jahn-Teller distortion. In Co-DOTAH$_2$ the equatorial Co-N bond length (2.171 Å) differs very little from the axial (2.203 Å). This is contrary to the Jahn-Teller distorted Cu-DOTA (Cu-N_{eq} = 2.107 Å; Cu-N_{ax} = 2.318 Å).

Temperature-dependent ^{1}H NMR studies of Co-DOTA and Co-DOTA-D-PheNH$_2$, in a large spectral window, revealed that the number of signals and their width can vary significantly, reflecting a combination of paramagnetic shift and exchange effects, consistent with a high spin state for the Co^{II} ion.

Our results demonstrate that dioxygen does not oxidise these polyamine polycarboxylate cobalt chelates despite the fact that the experiments were carried out in aerated solutions. This is in accordance with earlier reports that tertiary amine ligands stabilise low valent transition metal ions, in particular the Co^{II} ion[25, 26].

The thermodynamic stability of Co^{II}-DOTATOC was estimated by assessing the thermodynamic stability of the model chelate Co^{II}(DOTA-D-Phe-NH_2)$^-$. For this purpose we performed complexation competition experiments using $^{57}Co^{II}$ as radiotracer and DOTA as an auxiliary competing ligand. The integration of the HPLC-radiochromatographic peaks corresponding to $^{57/59}$Co(DOTA)$^{2-}$ and $^{57/59}Co^{II}$(DOTA-D-Phe-NH_2)$^-$ (Figure 2) remains unchanged after equilibration and allows the estimation of the conditional stability constant of Co^{II}(DOTA-D-Phe-NH_2)$^-$ at different pH values.

((Insert Figure 2 here))

Figure 2. Typical HPLC-radiochromatogram of a 1:1:1 mixture of $^{57,59}CoCl_2$:DOTA:DOTA-D-PheNH_2 (0.1 M NaOAc, pH 5.0) after 9 days of incubation at RT.

This method requires the knowledge of the stability constant of Co^{II}(DOTA)$^{2-}$ (log$K_{Co(DOTA)}$=19.9) and of the protonation constants of both ligands. Using the relationships $K_{cond}=\alpha K_{ML}$;

$$\alpha^{-1} = (1 + K_1[H^+] + K_1K_2[H^+]^2 + ... + K_n[H^+]^n)$$

(where K_1, K_2, K_n are the protonation constants of the free ligand); and

$$K_{rel} = \frac{[ML_2]\cdot[L_1]_t}{[ML_1]\cdot[L_2]_t} = \frac{K_{ML2}\cdot\alpha_{L2}}{K_{ML1}\cdot\alpha_{L1}}$$

we were able to estimate the thermodynamic stability constant of Co^{II}(DOTA-D-PheNH_2)$^-$ to logK_{ML}=19.6. This value shows that the model peptide chelate does not undergo a significant loss of thermodynamic stability compared to that of Co^{II}(DOTA)$^{2-}$.

Potentiometry allowed obtaining the protonation constants (pK_a´s) of DOTA and DOTA-D-PheNH_2; DOTA: pK_1=12.32(6), pK_2=9.73(1), pK_3=4.60(1), pK_4=4.06(2), and pK_5=2.08(9); DOTA-D-PheNH_2: pK_1=11.63(14), pK_2=9.28(5), pK_3=4.18(14), pK_4=2.14(16) and pK_5<2 (μ=0.5 M tetramethylammonium nitrate, 25°C). The lower protonation constants of DOTA-D-PheNH_2, in comparison to those of DOTA, arise from the charge difference of the two chelators.

The kinetic stability of [^{57}Co]DOTATOC in regard to trans-chelation was evaluated in the presence of 10^4 times excess of DTPA (acetate buffer, pH 5.0). The chemical inertness of the radiometal-labelled peptide was also studied measuring the isotope exchange rate in the presence of a 10^4-fold excess of free $^{59}Co^{II}$. The results showed high stability of [^{57}Co]DOTATOC over a time interval of 7 days (>98% intact radiopeptide).

In human serum the iron transport protein transferrin can bind with high affinity to many metal ions including Co^{II},[27] in this respect it is important to evaluate the kinetic stability of radiometal-labelled peptides under physiological conditions. For this purpose we measured the rate of $^{57}Co^{II}$ transfer from [^{57}Co]DOTATOC in human blood serum.[28] The approximate transfer half-life is 800 h, which compares to$T_{1/2}$=1250 h of [^{67}Ga]DOTATOC[13].

Receptor binding assays

Table 1 shows the IC_{50} values of Co^{II}-DOTATOC, compared to other somatostatin-based metallopeptides for the five somatostatin receptor subtypes (sst1-sst5). SS28 (somatostatin 28) was the control peptide. These values were obtained performing a competition experiment with the cold $^{59}Co^{II}$-labelled peptide and the universal somatostatin radioligand ^{125}I-[Leu^8,D-Trp^{22},Tyr^{25}]-SS28 on cell membranes expressing the different receptor subtypes. Co^{II}-DOTATOC exhibits circa 6 times higher affinity to sst2 than SS28, whereas Ga^{III}-DOTATOC is equipotent and Y^{III}-DOTATOC has a fourfold lower sst2-affinity than SS28. Co^{II}-DOTATOC shows the highest sst2 affinity of any somatostatin-based metallopeptide found so far.[12] Additionally, Co^{II}-DOTATOC shows also higher affinity to sst4 than the other two metallopeptides but a distinctly lower sst5 affinity.

Table 1. Affinity profiles (IC_{50}) for human sst1-sst5 receptors for different somatostatin analogues

Compound	sst1	sst2	sst3	sst4	sst5
SS-28 [a]	5.2±0.3 (19)	2.7±0.38 (19)	7.7±0.9 (15)	5.6±0.4 (19)	4.0±0.3 (19)
Octreotide [a]	>10000 (5)	2.0±0.7 (5)	187±55 (3)	>1000 (4)	22±6 (5)
Y^{III}-DOTATOC [a]	>10000 (4)	11±1.7 (6)	389±135 (5)	>10000 (5)	114±29 (5)
Co^{II}-DOTATOC	>10000 (5)	0.44±0.1 1 (5)	>1000 (5)	610±258 (4)	440±132 (5)
Ga^{III}-DOTATOC [a]	>10000 (6)	2.5±0.5 (7)	613±140 (7)	>1000 (6)	73±21 (6)

[a] data from Reubi et al.[12]

Internalisation and efflux

The specific internalisation of [^{57}Co]DOTATOC was evaluated using AR4-2J rat pancreatic tumour cells which exclusively express sst2. The radiometal-labelled peptide showed a time-dependent uptake with a very high specific internalisation rate, as shown in Figure 3 (scale of left y-axis and lower x-axis).

((Insert Figure 3 here))

Figure 3. Internalisation (triangles; scales on the left side and bottom) and externalisation (diamonds; scales on the right side and top) of [^{57}Co]DOTATOC in rat pancreatic AR4-2J cells.

After 6 h [^{57}Co]DOTATOC showed almost 50% specific internalisation in 1 million cells, constituting the highest internalisation rate ever found for a somatostatin derivative. In the same cell line [^{67}Ga]DOTATOC showed an uptake of 16.5±1% at 4 h p.i.[29]; [^{57}Co]DOTATOC internalised about 30% at 4 h p.i. whereas [^{111}In]DOTATOC internalised 11.5±0.7% of the total amount of radiopeptide added to 1 million cells. In order to evaluate the retention of the radiometal-peptide in the tumour cells, externalisation experiments were performed also in AR4-2J tumour cells. Cells were pre-loaded with [^{57}Co]DOTATOC for 2 h at 37°C. To remove the receptor-bound radiometal-peptide an acid

wash was carried out twice with a 0.1 M glycine buffer pH 2.8, 10 min, on ice. Afterwards, externalisation of [^{57}Co]DOTATOC was monitored at 30, 60, 120 and 240 min at 37°C, as shown in Figure 3 (scale of right y-axis). The externalisation results also showed a time dependence: the radiometal-labelled peptide presented circa 40% efflux from the cells within 4 h.

Biodistribution in tumour-bearing mice

For comparative reasons pharmacokinetic studies were performed in two mouse models (nude mice bearing the AR4-2J or HEK-sst2 tumour [30, 31]. The results are given in Tables 2 and 3 and in Figure 4 as % of injected activity per gram of tissue (% IA/g).

((Insert Figure 4 here))

Figure 4. Biodistribution of [^{57}Co]DOTATOC in nude mice bearing a tumour (% IA/g: % injected activity per gram).

The radiometal-labelled peptide was cleared rapidly from the circulation as demonstrated by the measurement of blood samples taken at 4, 24, and 48 hours p.i. (AR4-2J) or 0.5, 1, and 4 hours p.i. (HEK-sst2).

Table 2. Biodistribution of [^{57}Co]DOTATOC in a nude mouse tumour-bearing (AR4-2J) animal model (4, 24 and 48 h p.i.).

Organ	4 h unblocked	4 h blocked	24 h	48 h
Blood	0.03±0.01	0.06±0.03	0.01±0.00	0.01±0.00
Pancreas	2.81±0.60	0.62±0.31	0.25±0.05	0.11±0.04
Small intestine	0.69±0.34	0.27±0.11	0.21±0.02	0.08±0.02
Spleen	0.11±0.22	0.12±0.04	0.07±0.02	0.03±0.00
Liver	0.20±0.02	0.39±0.13	0.07±0.02	0.07±0.03
Stomach	5.75±0.80	1.65±0.54	2.56±0.26	1.37±0.33
Adrenals	2.33±0.54	0.75±0.15	2.20±0.43	1.33±0.41
Kidneys	9.11±2.24	22.88±6.86	1.24±0.38	1.38±0.65
Lung	0.34±0.06	0.41±0.15	0.06±0.03	0.05±0.02
Heart	0.06±0.01	0.07±0.02	0.03±0.01	0.02±0.00
Tumour	22.81±2.88	8.52±1.71	2.08±0.41	0.70±0.25
Tumour/non-tumour-ratios				
Tumour/blood	760		208	70
Tumour/liver	114		397	10
Tumour/kidney	2.5		2.01	0.51

Less than 0.15% IA/g remained in blood after 4 h. The clearance from all somatostatin receptor-negative tissues including the kidneys is also fast. Unexpectedly, also the tumour uptake in the AR4-2J tumour decreased between 4 h and 24 h by >90%. This was never observed before in any somatostatin-based radiopeptide which usually show biological half-lives of ≥24 h in tumours of this tumour model[30]. The highest tissue activity was found in the kidneys, which demonstrates the renal excretion of the radiopharmaceutical. At all time points the uptake in other organs was considerably lower except for the stomach which has been known for its presence of somatostatin receptors. Some uptake could be seen in the pancreas and the adrenals as well, which was expected since these two organs express somatostatin receptors. The pancreas shows a good clearance after 24 h whereas the uptake in the adrenals stays relatively high (60% of the 4 h value after 48 h).

Table 3. Biodistribution of [^{57}Co]DOTATOC in a nude mouse model (HEK-sstr2); 0.5 h, 1 h, 4 h, 4 h blocking)

Organ	0.5 h	1 h	4 h	4 h blocking
Blood	1.56±0.16	0.48±0.23	0.13±0.02	0.12±0.06
Heart	0.84±0.02	0.32±0.03	0.19±0.01	0.07±0.02
Liver	1.24±0.05	0.69±0.01	0.40±0.04	0.83±0.11
Spleen	0.96±0.22	0.67±0.15	0.34±0.04	0.36±0.18
Lung	2.29±0.17	6.37±2.74	1.24±1.05	0.29±0.06
Kidneys	16.80±2.20	12.15±2.14	6.48±0.62	8.81±0.73
Stomach	21.13±9.09	17.10±0.96	8.24±1.29	0.55±0.47
Intestine	1.88±0.05	2.18±0.63	1.07±0.20	0.21±0.21
Adrenals	2.78±0.38	1.35±0.08	1.58±0.49	0.18±0.14
Pancreas	28.86±0.47	15.36±0.54	5.44±2.13	0.34±0.37
Pituitary	5.80±2.90	9.47±1.93	4.56±2.86	0.25±0.09
Muscle	0.82±0.70	0.16±0.03	0.07±0.03	0.19±0.29
Tumour	28.35±2.46	28.97±3.85	34.91±0.23	5.15±0.79
Tumour/Non-Tumour Ratios				
Tumour/Blood	18	60	278	
Tumour/Liver	23	42	86	
Tumour/Kidney	1.7	2.4	5.4	

A high radioligand accumulation could be measured in the tumours four hours after the injection. When the receptors were blocked by a simultaneous injection of octreotide the accumulation of radioactivity in the tumour was significantly reduced by 63%. A higher reduction could be seen in the stomach (71%), the pancreas (88%), and the adrenals (68%). Upon blocking the accumulation in the kidneys was increased by a factor of 2.5.

In all non-tumour and non-receptor-specific tissues a fast clearance of the radiopharmaceutical was observed; this even holds for the kidneys (after 48 h 15% of the activity of the 4 h value is found in this organ).

The HEK-sst2 model was used to study the pharmacokinetics at shorter time points for comparative reasons. The general picture was similar to the other tumour model. The tumour uptake was very high, doubling the value obtained using another potent sst2-selective radiopeptide, [^{111}In]DTPA-TATE (IC_{50} = 1.3 nM) at 4 h p.i. [31]. Blocking was performed by coinjection of 100 µg [DOTA,Tyr^3,Thr^8]octreotide (DOTATATE) and was more efficient than the blocking with 50 µg octreotide in the AR4-2J mouse model. The unspecific level was lowered to 14.7% in the tumour, 6.3% in the pancreas and 5.5% in the pituitary. The tumour uptake is persistent, even increasing, in the first 4 h whereas the initial high pancreas uptake is washing out relatively fast. The tumour/blood, tumour/liver and tumour/kidney ratios increased considerably during the first 4 hours and a value of 5.4 was never before observed in this or a similar tumour model using a somatostatin-based radiometallopeptide.

Coordination chemical aspects: It is of major importance to understand why the radiometal ion influences the receptor binding affinity and the tumour uptake. With regard to this we crystallised two model chelates,

$Co^{II}(H_2DOTA)$ and $Ga^{III}(DOTA)^-$, which correspond respectively to the metal chelate moieties of Co^{II}-DOTATOC and Ga^{III}-DOTATOC, and determined their X-ray structures. Both chelates crystallise as diprotonated species. ORTEP representations of the chelates are shown in Figures 5 and 6. Crystallographic data are summarised in Table 4.

((Insert Figure 5 here))

Figure 5. Ortep plot of the crystal structure of $Co^{II}(DOTA)^{2-}$ (thermal ellipsoids at 50% probability level). Selected bond lengths [Å] and angles [°]: Co(1)-N(2) 2.271(6), Co(1)-N(2) 2.271(6), Co(1)-N(3) 2.203(6), Co(1)-N(3) 2.203(6), Co(1)-O(5) 2.038(5), Co(1)-O(5) 2.038(5); N(2)-Co(1)-N(2) 108.1(3), N(3)-Co(1)-N(3) 154.0(3), O(5)-Co(1)-O(5) 90.7(3).

((Insert Figure 6 here))

Figure 6. Ortep plot of the crystal structure of $Ga^{III}(DOTA)^-$ (thermal ellipsoids at 50% probability level). Selected bond lengths [Å] and angles [°]: Ga(1)-N(3) 2.105(9), Ga(1)-N(5) 2.116(9), Ga(1)-N(2) 2.116(10), Ga(1)-N(4) 2.187(10), Ga(1)-O(8) 1.940(7), Ga(1)-O(12) 1.913(8); N(3)-Ga(1)-N(5) 109.0(2), O(12)-Ga(1)-O(8) 82.39(13), N(2)-Ga(1)-N(4) 157.1(2).

Table 4. Crystallographic data of $Co^{II}(DOTA)^{2-}$ and $Ga^{III}(DOTA)^-$ chelates

	$Co^{II}(H_2DOTA)$	**$Ga^{III}(H_2DOTA)^+Cl^-$**
chem. formula	$C_{16}H_{26}CoN_4O_8$	$C_{16}H_{26}ClGaN_4O_8.5H_2O$
fw	461.34	597.65
cryst. size /mm	0.6x0.6x0.4	0.5x0.5x0.5
space group	Pccn	C_C
cryst. syst.	orthorhombic	monoclinic
a/Å	15.225 (3)	15.171,90
b/Å	9.3920 (19)	14.962,94.10
c/Å	13.065 (3)	10.068,90
V/Å^3	1868.2 (6)	2279.5
Z	4	4
ρ_{calcd}/g cm^{-3}	1.640	1.706
T/K	183(2)	183(2)
μ/mm^{-1}	0.974	1.400
λ̃Å	0.71073 ($Mo_{k\alpha}$	0.71073 ($Cu_{k\alpha}$

The structures of the Co^{II}- and Ga^{III}-DOTA chelates are very similar showing six-coordination and a pseudooctahedral geometry. Axially, two macrocyclic ring nitrogens and two trans-arranged carboxylate oxygens are bound whereas the remaining two ring nitrogens form equatorial bonds to the metals. The deviation from the octahedron is seen in the equatorial N-M-N bond angles (180° in a regular octahedron) of 154° and 157° for $Co^{II}(H_2DOTA)$ and $Ga^{III}(H_2DOTA)^+$, respectively. Table 5 shows some selected bond lengths, angles and planes of both chelates. The two structures are almost identical and close to the corresponding structure of Ga^{III}(DOTA-D-$PheNH_2$)[13] showing the relevance of the structures to the monoamide peptide derivatives. In both structures, as in Ga^{III}(DOTA-D-$PheNH_2$), the macrocyclic unit adopts a 2424 conformation. The somewhat smaller bond lengths in $Ga^{III}(H_2DOTA)^+$, relative to $Co^{II}(H_2DOTA)$, are compatible with a metallic centre of higher charge density (ionic radius of Ga^{3+}=62 pm; ionic radius of $Co^{2+}_{high\ spin}$=73.5 pm).

Table 5. Selected average bond lengths [Å], angles [°] and planes of $Co^{II}(DOTA)^{2-}$ and $Ga^{III}(DOTA)^-$ chelates.

		$Co^{II}(H_2DOTA)$	$Ga^{III}(H_2DOTA)^+$
CN [a]		6	6
Ring config.		2424	2424
M-N [Å]	eq	2.171 (6)	2.111 (8)
	ax	2.203 (6)	2.152 (50)
N-M-N [°]	eq	154.0 (3)	157.1 (2)
	ax	108.1 (3)	109.0 (2)
O-M-O [°]	eq	90.7 (3)	82.39 (2)
M-O [Å]	eq	2.038 (5)	1.927 (19)
D_{N2O2} [Å]		0.037	0.068
R_{N2O2} [Å]		0.08	0.005

[a] CN is the coordination number of the metal ion, D_{N2O2} is the distance to the plane, R_{N2O2} is the distance of the defining atoms to the best plane (P_{N2O2}).

Like in Ga^{III}(DOTA-D-$PheNH_2$)[13], $Ga^{III}(H_2DOTA)^+$ and $Co^{II}(H_2DOTA)$ only show coordination of two acetate groups whereas the remaining two are free and one of them will always be used when the chelator is coupled to a biomolecule forming an amide bond. The similar structural features of $Co^{II}(H_2DOTA)$ and $Ga^{III}(H_2DOTA)^+$ allow the assumption that [^{57}Co]DOTATOC and [^{67}Ga]DOTATOC might also have similar structures and consequently one would expect the two radiopeptides to have similar biological behaviour. The fact that in both radiopeptides one carboxylate group is free and deprotonated at physiological pH contributes to their fast and efficient clearance through the kidneys. Despite the likely structural similarities of [^{57}Co]DOTATOC and [^{67}Ga]DOTA-TOC, the two radiopeptides show remarkably different biological behaviour, which we tend to assign to the different charge density of the metal ions.

Conclusion

[^{57}Co]DOTATOC and [^{67}Ga]DOTATOC are two radiopharmaceuticals which, despite their structural similarities (as shown by the X-ray structures of the model chelates $Co^{II}(H_2DOTA)$ and $Ga^{III}(H_2DOTA)^+$) display different biological behaviour. [^{57}Co]DOTATOC presents the highest affinity for the sst2 subtype receptor of any radiometal-labelled somatostatin derivative. The improved receptor binding affinity is reflected in a high and specific tumour uptake and a high rate of internalisation. [^{57}Co]DOTATOC has a relatively short tumour residence time in the AR4-2J animal model. This may not be a disadvantage if similar in humans as it leads to a low patient dose. In addition, its tumour-to-kidney ratio is one of the highest of any radiopeptide of the somatostatin analogues.

Cobalt in [^{57}Co]DOTATOC is present in the oxidation state of +2, as demonstrated in aqueous solutions of $Co^{II}(H_2DOTA)$ and Co^{II}(DOTA-D-$PheNH_2)^-$, and the coordination geometry of the Co^{II} ion is a somewhat distorted octahedron.

This work illustrates how the physical features (size, charge) of the radiometal strongly influence the receptor affinity, biodistribution and pharmacokinetics of radiometal labelled peptides. Our results encourage further animal and

possibly clinical studies in order to evaluate the full potential of [^{55}Co]DOTATOC as a PET agent.

Experimental Section

Chemicals and analysis: All chemicals were obtained from commercial sources and used without further purification. DOTA was a gift from Guerbet, France. $^{57}CoCl_2$ was purchased from Isotope Products Laboratories, Burbank (CA), USA. Sephadex G-50 (Pharmacia) was used for gel chromatography. Electrospray ionisation (ESI) was carried out with a Finnigan SSQ 7000 spectrometer. Analytical and semipreparative HPLC was performed on a Hewlett Packard 1050 HPLC system with a multiwavelength detector and a flow through Berthold LB 506 C1 γ-detector. Quantitative γ-counting was performed on a COBRA 5003 γ-system well counter from Packard Instrument Company. $^{1}H/^{13}C$ NMR was performed with either a Varian VXR 400 at 400/101 MHz or a Varian Unity 500 at 500/126 MHz. Chemical shifts reported are relative to TMS. ^{59}Co NMR was performed on a Bruker AV400 spectrometer at 94.939 MHz; 0.1 M $K_3[Co(CN)_6]$ in D_2O was used as an external reference and the presence of signals was checked between +15000 and -1000 ppm.

Syntheses and labelling

[DOTA^0,Tyr^3]-octreotide (DOTATOC) and Ga^{III}-DOTATOC were synthesised as described previously[13].

[^{57}Co]DOTATOC: [^{57}Co]DOTATOC was prepared as follows: DOTATOC (10 µg, 7 nmol) was dissolved in a sodium acetate buffer (20 µL, 0.4 M, pH 5.0). $^{57}CoCl_2$ (43 µCi) was added and the mixture heated at 95°C for 30 min. Quality control was performed with HPLC (Nucleosil 120-C18, M&N; eluents A = 0.1% TFA in H_2O and B = CH_3CN; gradient: 0-5 min 100% A, 25 min 75% A, 30-35 min 100% A). The labelling yield was >99.5%; the achieved specific activity was 5 mCi/µmol, which corresponds to a peptide-to-^{57}Co ratio of 50:1. MS-ESI: *m/z* = 1477.3 $[M-H]^-$ (100%), 1499.5 $[M+HCOO^-]^-$ (20%), 1535.8 $[M+CH_3COO^-]^-$ (10%); purity (HPLC): > 97%.

Co^{II}(DOTA-D-PheNH$_2$)$^-$: Co^{II}(DOTA-D-PheNH$_2$)$^-$ was obtained from the reaction of DOTA-D-PheNH$_2$ (8.0 mg, 14.5 µmol) with $CoCl_2 \cdot 6\ H_2O$ (3.8 mg, 16 µmol) in aqueous solution (1 ml, pH 4, 95°C, 30 min). After cooling to room temperature the pH was adjusted to 5 with 0.1 M NaOH. Evaporation to dryness afforded a purple solid in quantitative yield. MS-ESI: $C_{25}H_{36}CoN_6O_8$ (M = 607.52 g/mol) *m/z* = 608.8 $[M+H]^+$ (30%); 630.5 $[M+Na]^+$ (20%); 606.4 $[M-H]^-$ (100%); ^{1}H NMR (500 MHz, 25°C, D_2O): δ = 6.9 (s, br, 2 H arom. ortho), 7.7 (m, 2 H arom. meta and 1 H arom. para); in the 2.25 – 3.25 ppm range one detects three small broad signals (each one with an integration corresponding to 1 H). We checked for ^{1}H NMR signals in a spectral window of +400 to –400 ppm in the temperature range 5-90 °C. ^{59}Co NMR spectroscopy (94.939 MHz, 25 °C, D_2O) showed no signals in a spectral window of +15000 to –1000 ppm.

Co^{II}(H$_2$DOTA): Co^{II}(H$_2$DOTA) was obtained from the reaction of DOTA (50 mg, 0.12 mmol) with $CoCl_2 \cdot 6\ H_2O$ (28.6 mg, 0.12 mmol) in aqueous solution (5 ml, pH 4.8, 95°C, 25 min). Slow evaporation produced light red single crystals suitable for X-ray analysis. MS-ESI: $C_{16}H_{26}CoN_4O_8$ (M = 461.11 g/mol) *m/z* = 462.1 $[M+H]^+$ (100%); ^{1}H NMR (400 MHz, 25°C, D_2O): no signals were observed.

Ga^{III}(H$_2$DOTA)$^+$Cl$^-$: Ga^{III}(H$_2$DOTA)$^+$Cl$^-$ was obtained from the reaction of DOTA (78.73 mg, 0.181 mmol) with $Ga(NO_3)_3 \cdot 9\ H_2O$ (91 mg, 0,217 mmol) in aqueous solution (5 ml, pH 4, 80°C, 30 min). After cooling at room temperature, the pH was adjusted to 8 with 0.1 M NaOH. Excess of Ga^{III} (in the form of hydroxide) was filtered off and the final pH adjusted to 7 with 0.1 M HCl. Slow evaporation of water afforded colourless crystals suitable for X-ray diffraction. MS-ESI: $C_{16}H_{25}GaN_4O_8$ (M = 471.11 g/mol), *m/z* = 471.1, 472.1(6:4) $[M+H]^+$ (100%); Elemental analysis**:** $C_{16}H_{25}N_4O_8Ga \cdot HNO_3 \cdot 2H_2O$ (M = 570.16 g/mol): theoretically C 33.71, H 5.30, N 12.29, O 36.47; found C 33.57, H 5.10, N 12.25, O 31.52; ^{1}H-NMR: (400 MHz, 27°C, D_2O): δ = 3.40 (s, br, 16 H, N-CH_2-CH_2-N), 3.68 (s, br, 8 H, N-CH_2-COOD); ^{13}C-NMR: (101 MHz, 27°C, D_2O, pD = 6.9): δ = 52.52 (N-<u>C</u>H$_2$-<u>C</u>H$_2$-N), 58.48 (N-<u>C</u>H$_2$-COOGa), 176.40 (<u>C</u>OOGa); IR (KBr): ν = 3570, 3492, 2956, 2705, 2650, 2590, 1746, 1710, 1699, 1620, 1496, 1475, 1384, 1339, 1316, 1287, 1240, 1212, 1083, 1047, 925 cm^{-1}.

Kinetic exchange

The kinetic stability of [^{57}Co]DOTATOC upon trans-chelation was determined using a 10^4-fold excess of DTPA. [^{57}Co]DOTATOC (6 µL, 10^{-11} mol) was mixed with DTPA (10 µl, 10^{-7} mol) and 484 µL 0.1 M NaOAc pH 5.0. The exchange rate of this solution was measured by taking aliquots (50 µL) and the exchange ratio [^{57}Co]DOTATOC versus ^{57}Co^{II}(DTPA)$^{3-}$ was analysed by HPLC at time intervals of 4 to 24 h.

In addition, the chemical inertness of [^{57}Co]DOTATOC was verified by measuring the isotope exchange rate of the radiocobalt-labelled peptide versus a 10^4 excess of free ^{59}Co^{II}. The experiment was carried out using similar concentrations of [^{57}Co]DOTATOC and $^{59}CoCl_2$ as described above. Aliquots of 50 µL were incubated with DTPA (10^{-3} M, 10 µL) prior to HPLC analyses to enable a detection of ^{57}Co^{II} as [^{57}Co](DTPA)$^{3-}$ complex.

Serum stability studies

[^{57}Co]DOTATOC was added to fresh human blood serum (1 µCi/mL) and incubated at 37°C in a CO_2 atmosphere (5%). At defined times aliquots of 50-100 µL were taken and analysed by gel-chromatography (Sephadex G50, PBS buffer 0.01 M, pH 7.4). Low- and high-molecular fractions were collected and measured with a γ-counter. The amount of serum protein-bound radiopeptide was calculated by the count rates of both fractions [32].

Thermodynamic stability and protonation constants

The thermodynamic stability constant of Co^{II}(DOTA-D-PheNH$_2$)$^-$ was estimated by competition experiments using DOTA as a competing chelator. For this purpose, solutions containing similar amounts of both ligands were used (0.01 M, 40 µL). $^{57/59}CoCl_2$ was added in phosphate-buffer (0.01 M, pH 7.0, 20 µL). The mixture was incubated at room temperature at controlled pH. Aliquots of 15 µL were taken at different times and analysed by HPLC equipped with a Berthold γ-detector (CC 250-4 mm 120-3 C_8, M&N, eluent: A = 0.1% TFA in H_2O, B = CH_3CN, 0-5 min 100% A, 25-35 min 30% B, 35 min 100% A).

The protonation constants of DOTA and DOTA-D-Phe-NH$_2$ were obtained by potentiometric titration in a thermostated cell at 25°C under a stream of N_2 with a 0.5 M solution of tetramethylammonium hydroxide (standardised with potassium hydrogenophtalate) at an ionic strength adjusted to 0.5 M with tetramethylammonium nitrate in a Metrohm 665-Dosimat equipped with a 1 mL piston burette. Excess nitric acid was added to the ligand solutions to determine the lower protonation constants. All the solutions were prepared with deionised water (Millipore) which was previously boiled to remove the CO_2. pH measurements were carried out with a Metrohm 645 digital pH-meter equipped with a Metrohm 6.0204.100 glass electrode combined with a calomel (3 M KCl) reference electrode. The glass electrode was calibrated with pH 4.0 and 7.0 buffers at 25°C. The pH meter/electrode system was calibrated by titration of a 3.2 mM TRIS solution with 0.5 M tetramethylammonium hydroxide at an ionic strength adjusted to 0.5 M with tetramethylammonium nitrate. The data were handled and calculated with the program TITFIT[33].

Cell culture

AR4-2J rat pancreatic tumour cells expressing sst2 were cultured in high glucose Dulbecco's minimal essential medium (DMEM), enriched with 4 nM glutamine, 10% FBS, amino acids, vitamins and penicillin-streptomycin from BioConcept (Allschwil, Switzerland). Cells were maintained in a humidified 5% CO_2/air atmosphere at 37°C. The viability of the cells was assessed using trypan blue stain and counted under a microscope with a "Neubauer's counting chamber".

Receptor binding assays

Cells stably expressing human sst1, sst2, sst3, sst4 and sst5 were grown as described previously[12]. All culture reagents were supplied by Gibco and Life Technologies (Grand Island, NY). Cell membrane pellets were prepared and receptor autoradiography was performed on pellet sections (mounted on microscope slides), as described in detail previously [12].

Complete displacement experiments were performed with the universal somatostatin radioligand ^{125}I-[Leu^8,D-Trp^{22},Tyr^{25}]-somatostatin-28 (2000 Ci/mmol; Anawa, Wangen, Switzerland), using increasing concentrations of the unlabelled peptide ranging from 0.1 to 1000 nM. Somatostatin-28 was run in parallel as control using the same increasing concentrations. IC_{50}-values (inhibitory concentration 50%) were calculated after quantification of the data using a computer-assisted image processing system. Tissue standards (autoradiographic [^{125}I]microscales, Amersham, UK) containing known amounts of isotopes, cross calibrated to tissue-equivalent ligand concentrations, were used for quantification[12]. The peptide concentration was measured by UV spectroscopy (ε_{280nm} = 6849), according to the method of Reubi[12], and was based on the exact knowledge of the elemental analysis of [DOTA^0,Tyr^3]-octreotide.

Internalisation and efflux studies

Cells (10^6/well) were distributed in six-well plates at 37°C, in a 5% CO_2/air atmosphere during one night in culture medium (DMEM with 10% FBS). The medium was removed; the cells were washed and incubated for 1 h, with internalisation medium (DMEM with 1% FBS) under the same conditions as described above. Approximately 0.02 MBq/well of the radioligand (2.5 pmol/well) were added to the medium and the cells were incubated at 37°C, 5% CO_2, with and without excess of peptide (1 µg) to determine non-specific internalisation. At appropriate time periods, the internalisation was stopped by removing the medium and washing the cells with ice cold PBS. To remove the receptor-bound radioligand an acid wash was carried out with a 0.1 M glycine buffer pH 2.8, during 10 min, on ice. This procedure permits to distinguish between membrane-bound (acid-releasable) and internalised radioligand (acid-resistant). Finally, cells were solubilised with 1 M NaOH and incubated for 10 min at 37°C. The

radioactivity of the culture medium, the receptor-bound and the internalised fractions were measured in a γ–counter (Cobra II, Packard Instr., Switzerland).
For externalisation experiments the AR4-2J cells (10^6/well) were incubated with 2.5 pmol/well of radioligand. After 2 h of internalisation at 37°C, 5% CO_2, the medium was removed and the cells were washed twice with cold PBS. An acid wash was performed, as described in the previous section. Three millilitres of internalisation medium were added to each well and the cells were incubated at 37°C. At different time points the external medium was collected and exchanged with 37°C fresh medium. Thereafter, the cells were treated with 1 M NaOH to extract the internalised radioligand. The radioactivity of the external medium and of the internalised radioligand fractions was quantified in a γ–counter. The recycled fraction was expressed as percentage of the totally internalised amount per 1 million cells.

Biodistribution studies in tumour-bearing animals

All animal experiments were performed in compliance with the Swiss laws on animal protection (approval no. 789). Male nude mice (IFFACREDO, France) were injected subcutaneously in the right abdomen with a cell suspension of a rat pancreatic cell tumour (AR4-2J, 5 million cells/50 µL). Six to seven days post injection the tumours were grown to a size of approximately 0.5 cm in diameter. The animals were split into four groups: three batches of four animals without pre-treatment for 4 h, 24 h, and 48 h biodistribution studies; four animals which were injected with 50 µg Octreotide® together with the radiopharmaceutical. Both substances, the radioligand as well as Octreotide®, were prepared in a 0.1% bovine serum albumin solution in order to prevent sticking of the substances to the syringes. For the second tumour model five-week-old female Swiss athymic nude mice were implanted subcutaneously with 10 millions of HEK-sst2 cells on one flank. After 10-12 days the mice showed solid palpable tumour masses of 150-200 mg. In order to study the biodistribution of [^{57}Co]DOTATOC, 3 µCi (120±15 kBq) of the radioligand was injected by the tail vein as a bolus into the tumour-bearing mice. After the respective times the animals were sacrificed, a blood sample was taken, organs were removed, weighed, and the radioactivity was counted.

X-ray diffraction studies

The X-ray measurements of $Ga^{III}(DOTA)^-$ and $Co^{II}(DOTA)^{2-}$ were performed on a Nicolet P3 diffractometer with graphite-monochromatic $Mo_{K\alpha}$-radiation. Crystallographic data are summarised in Table 4, average bond lengths, angles and planes in Table 5. The structures were solved using Patterson methods, expanded by Fourier techniques and refined against F^2 by full-matrix least-squares methods using ShelX93 crystallographic software package[34]. Crystallographic data (excluding structure factors) for the structures of the gallium and the cobalt chelates have been deposited with the Cambridge Crystallographic Data Centre and allocated the deposition numbers CCDC 616729 & 616730, respectively. Copies of the data can be obtained free of charge on application to the director, CCDC, 12 Union Road, Cambridge CB2 1EZ, (fax: (+44) 1223-336-033, e-mail: deposit@ccdc.cam.ac.uk).

Acknowledgements

This work was supported by the Swiss National Science Foundation (project no. 320000-114043). J.P. André thanks the Foundation of Science and Technology (F.C.T.), Portugal, for the grant received during his sabbatical leave. Novartis (Basel, Switzerland) is acknowledged for the MS-ESI analysis. Kayhan Akyel is acknowledged for the ^{1}H NMR spectra. Dr. Maryse Bourdonneau (Bruker, Wissenbourg, France) is acknowledged for the ^{1}H and ^{59}Co NMR spectra. The authors are thankful to Daniel Storch for his help in the preparation of the figures for the manuscript.

[1] P. Blower, *Dalton Trans* **2006**, 1705-1711.

[2] S. Liu, *Chem Soc Rev* **2004**, *33*, 445-461.

[3] T. M. Behr, M. Gotthardt, A. Barth and M. Behe, *Q J Nucl Med* **2001**, *28*, 1421-1429.

[4] S. M. Okarvi, *Med Res Rev* **2004**, *24*, 357-397.

[5] M. Ginj and H. R. Maecke, *Met Ions Biol Syst* **2004**, *42*, 109-142.

[6] J. C. Reubi, *Endocr Rev* **2003**, *24*, 389-427.

[7] R. E. Weiner and M. L. Thakur, *BioDrugs* **2005**, *19*, 145-163.

[8] H. R. Maecke and J. P. Andre, *Ernst Schering Res Found Workshop* **2007**, 215-242.

[9] J. C. Reubi, H. R. Maecke and E. P. Krenning, *J Nucl Med* **2005**, *46*, 67S-75S.

[10] M. de Jong, W. A. Breeman, R. Valkema, B. F. Bernard and E. P. Krenning, *J Nucl Med* **2005**, *46 Suppl 1*, 13S-17S.

[11] D. J. Kwekkeboom, E. P. Krenning, W. H. Bakker, H. Y. Oei, P. P. Kooij and S. W. Lamberts, *Eur J Nucl Med* **1993**, *20*, 283-292.

[12] J. C. Reubi, J. C. Schar, B. Waser, S. Wenger, A. Heppeler, J. S. Schmitt and H. R. Maecke, *Eur J Nucl Med* **2000**, *27*, 273-282.

[13] A. Heppeler, S. Froidevaux, H. R. Mäcke, E. Jermann, M. Béhé, P. Powell and M. Hennig, *Chemistry A European Journal* **1999**, *5*, 1016-1023.

[14] D. J. Kwekkeboom, J. Mueller-Brand, G. Paganelli, L. B. Anthony, S. Pauwels, L. K. Kvols, M. O'Dorisio T, R. Valkema, L. Bodei, M. Chinol, H. R. Maecke and E. P. Krenning, *J Nucl Med* **2005**, *46*, 62S-66S.

[15] H. R. Maecke, M. Hofmann and U. Haberkorn, *J Nucl Med* **2005**, *46*, 172S-178S.

[16] M. de Jong, W. H. Bakker, E. P. Krenning, W. A. Breeman, M. E. van der Pluijm, B. F. Bernard, T. J. Visser, E. Jermann, M. Béhé, P. Powell and H. R. Maecke, *Eur J Nucl Med* **1997**, *24*, 368-371.

[17] M. Henze, A. Dimitrakopoulou-Strauss, S. Milker-Zabel, J. Schuhmacher, L. G. Strauss, J. Doll, H. R. Maecke, M. Eisenhut, J. Debus and U. Haberkorn, *J Nucl Med* **2005**, *46*, 763-769.

[18] K. Zhernosekov, P. Aschoff, D. Filosofov, M. Jahn, M. Jennewein, H. J. Adrian, H. Bihl and F. Rosch, *Eur J Nucl Med Mol Imaging* **2005**, *32*, 1129.

[19] H. M. Jansen, J. Pruim, A. M. vd Vliet, A. M. Paans, J. M. Hew, E. J. Franssen, B. M. de Jong, J. G. Kosterink, R. Haaxma and J. Korf, *J Nucl Med* **1994**, *35*, 456-460.

[20] H. Stevens, H. M. Jansen, J. De Reuck, M. Lemmerling, K. Strijckmans, P. Goethals, I. Lemahieu, B. M. de Jong, A. T. Willemsen and J. Korf, *J Neurol Sci* **1999**, *171*, 11-18.

[21] J. De Reuck, K. Paemeleire, P. Santens, K. Strijckmans and I. Lemahieu, *Clin Neurol Neurosurg* **2004**, *106*, 77-81.

[22] J. Korf, L. Veenma-van der Duin, R. Brinkman-Medema, A. Niemarkt and L. F. de Leij, *J Nucl Med* **1998**, *39*, 836-841.

[23] Z. Szabo, J. Xia, W. B. Mathews and P. R. Brown, *Semin Nucl Med* **2006**, *36*, 36-50.

[24] M. Ginj, J. S. Schmitt, J. Chen, B. Waser, J. C. Reubi, M. de Jong, S. Schulz and H. R. Maecke, *Chem Biol* **2006**, *13*, 1081-1090.

[25] G. Golub, H. Cohen and D. Meyerstein, *J Chem Soc Chem Comm* **1992**, 397-398.

[26] I. Bertini, L. Messori, G. Golub, H. Cohen and D. Meyerstein, *Inorg Chim Acta* **1995**, *235*, 5-8.

[27] T. A. Smith, *Bioorg Med Chem* **2005**, *13*, 4576-4579.

[28] G. Ruser, W. Ritter and H. R. Maecke, *Bioconjug Chem* **1990**, *1*, 345-349.

[29] P. Antunes, M. Ginj, H. Zhang, B. Waser, R. P. Baum, J. C. Reubi and H. Maecke, *Eur J Nucl Med Mol Imaging* **2007**, *34*, 982-993.

[30] S. Froidevaux, A. N. Eberle, M. Christe, L. Sumanovski, A. Heppeler, J. S. Schmitt, K. Eisenwiener, C. Beglinger and H. R. Maecke, *Int J Cancer* **2002**, *98*, 930-937.

[31] M. Ginj, H. Zhang, B. Waser, R. Cescato, D. Wild, X. Wang, J. Erchegyi, J. Rivier, H. R. Macke and J. C. Reubi, *Proc Natl Acad Sci U S A* **2006**, *103*, 16436-16441.

[32] A. Riesen, T. Kaden, W. Ritter and H. Maecke, *J Chem Soc Chem Comm* **1989**, 460.

[33] A. Zuberbuehler and T. Kaden, *Talanta* **1982**, *29*, 201-206.

[34] G. Sheldrick, *Acta Cryst* **1990**, *46*, 467-473.

Received: ((will be filled in by the editorial staff))
Revised: ((will be filled in by the editorial staff))
Published online: ((will be filled in by the editorial staff))

Legends to the figures

Figure 1. Structural formulae of [$DOTA^0$,Tyr^3]-octreotide (DOTATOC) (above) and DOTA-D-PheNH_2 (below).

Figure 2. Typical HPLC-radiochromatogram of a 1:1:1 mixture of $^{57,59}CoCl_2$:DOTA:DOTA-D-PheNH_2 (0.1 M NaOAc, pH 5.0) after 9 days of incubation at RT.

Figure 3. Internalisation (triangles; scales on the left side and bottom) and externalization (diamonds; scales on the right side and top) of [^{57}Co]DOTATOC in rat pancreatic AR4-2J cells.

Figure 4. Biodistribution of [^{57}Co]DOTATOC on nude mice bearing a tumour (% IA/g: % injected activity per gram).

Figure 5. Ortep plot of the crystal structure of $Co^{II}(DOTA)^{2-}$ (thermal ellipsoids at 50% probability level). Selected bond lengths [Å] and angles [°]: Co(1)-N(2) 2.271(6), Co(1)-N(2) 2.271(6), Co(1)-N(3) 2.203(6), Co(1)-N(3) 2.203(6), Co(1)-O(5) 2.038(5), Co(1)-O(5) 2.038(5); N(2)-Co(1)-N(2) 108.1(3), N(3)-Co(1)-N(3) 154.0(3), O(5)-Co(1)-O(5) 90.7(3).

Figure 6. Ortep plot of the crystal structure of $Ga^{III}(DOTA)^-$ (thermal ellipsoids at 50% probability level). Selected bond lengths [Å] and angles [°]: Ga(1)-N(3) 2.105(9), Ga(1)-N(5) 2.116(9), Ga(1)-N(2) 2.116(10), Ga(1)-N(4) 2.187(10), Ga(1)-O(8) 1.940(7), Ga(1)-O(12) 1.913(8); N(3)-Ga(1)-N(5) 109.0(2), O(12)-Ga(1)-O(8) 82.39(13), N(2)-Ga(1)-N(4) 157.1(2).

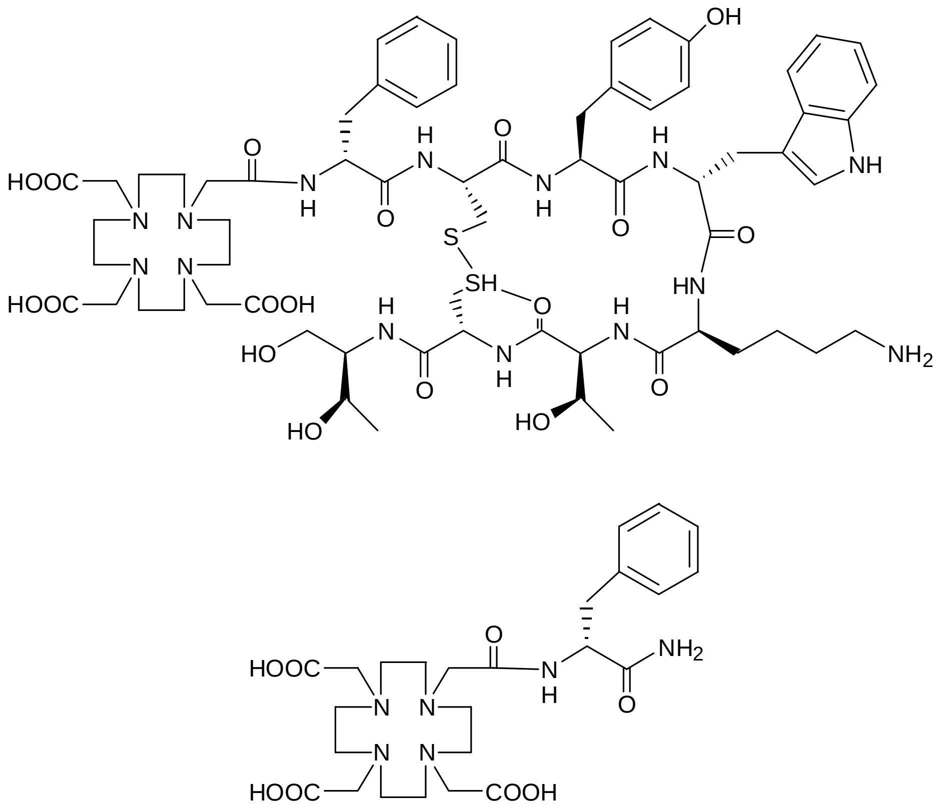

Figure 1. Structural formulae of [DOTA^{0},Tyr^{3}]-octreotide (DOTATOC) (above) and DOTA-D-PheNH_2 (below).

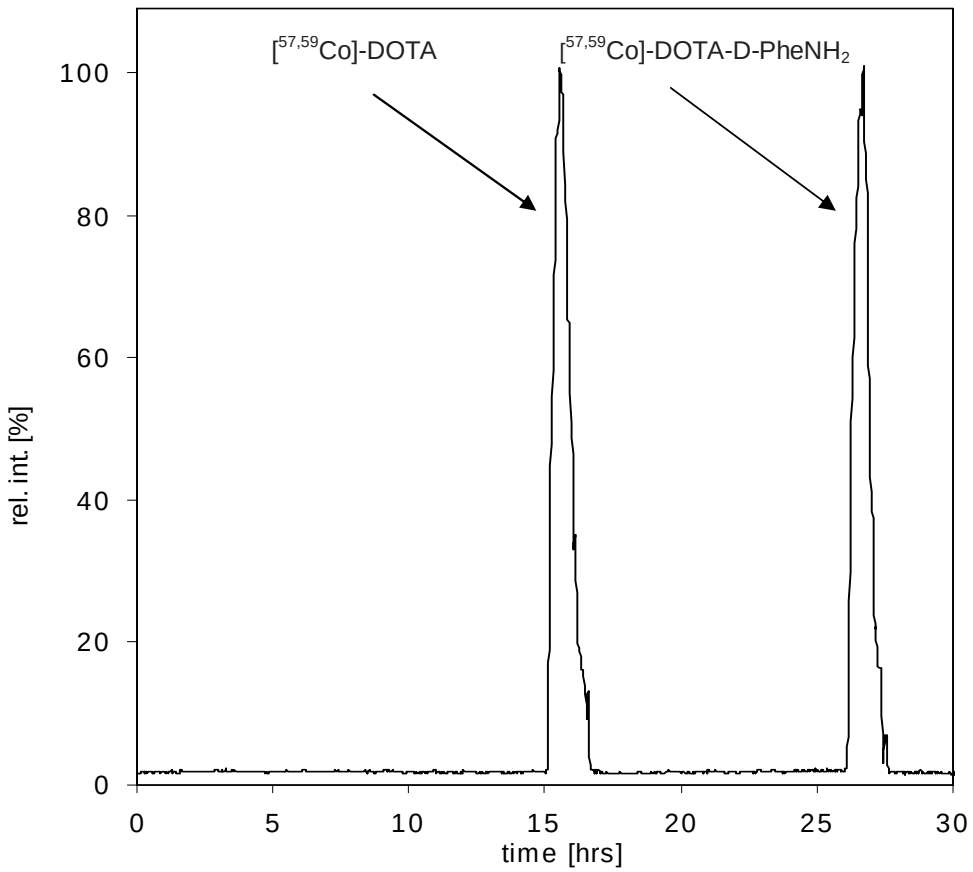

Figure 2. Typical HPLC-radiochromatogram of a 1:1:1 mixture of $^{57,59}CoCl_2$:DOTA:DOTA-D-PheNH_2 (0.1 M NaOAc, pH 5.0) after 9 days of incubation at RT.

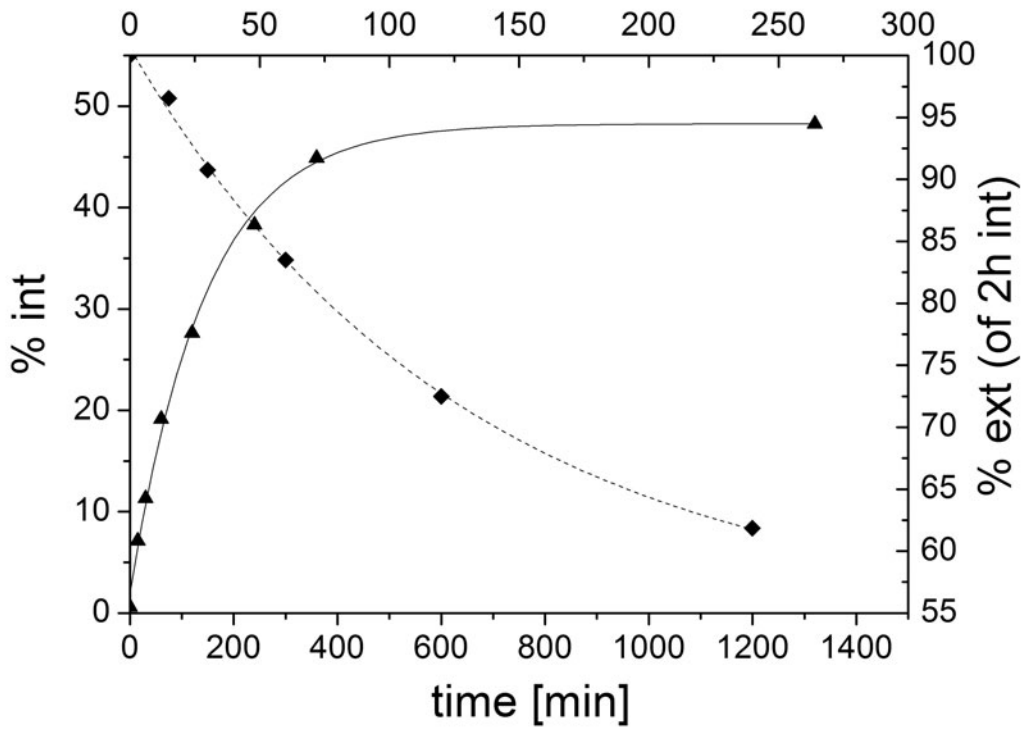

Figure 3. Internalisation (triangles; scales on the left side and bottom) and externalization (diamonds; scales on the right side and top) of [^{57}Co]DOTATOC in rat pancreatic AR4-2J cells.

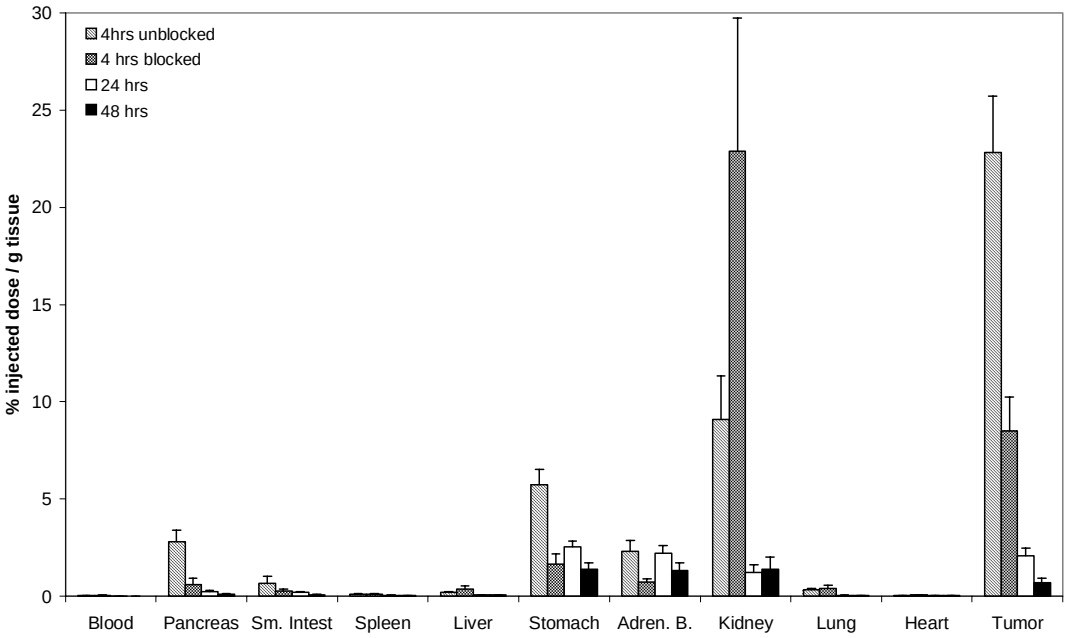

Figure 4. Biodistribution of [^{57}Co]DOTATOC on nude mice bearing a tumour (% IA/g: % injected activity per gram).

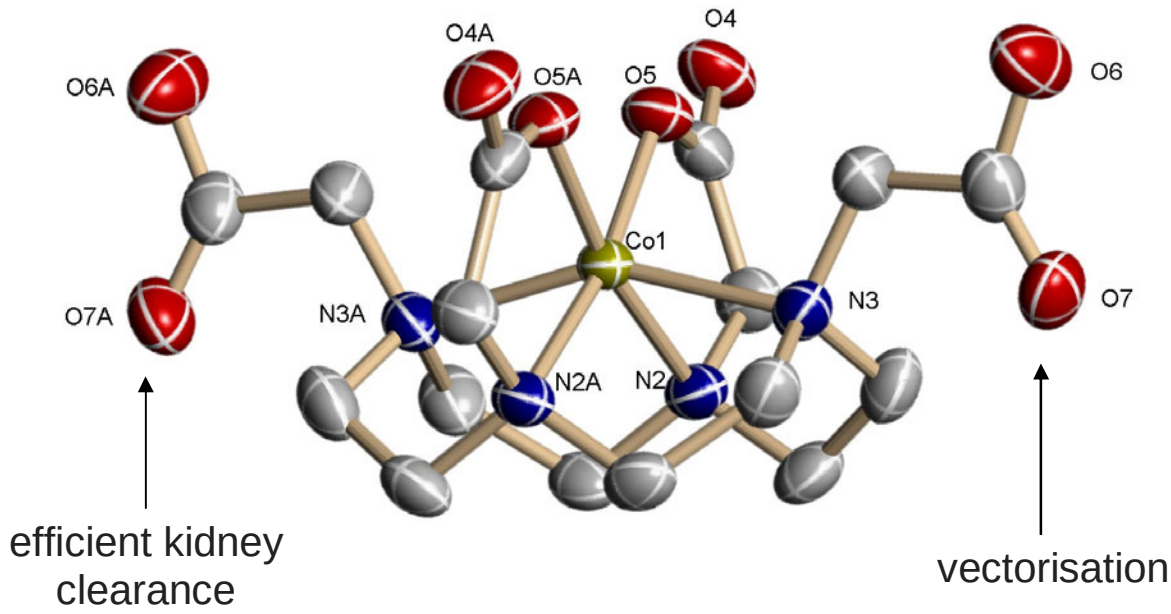

Figure 5. Ortep presentation of the X-ray structure $Co^{II}(DOTA)^{2-}$ (thermoparameter with 50% probability). Selected bond lengths [Å] and angles [°]: Co(1)-N(2) 2.271(6), Co(1)-N(2) 2.271(6), Co(1)-N(3) 2.203(6), Co(1)-N(3) 2.203(6), Co(1)-O(5) 2.038(5), Co(1)-O(5) 2.038(5); N(2)-Co(1)-N(2) 108.1(3), N(3)-Co(1)-N(3) 154.0(3), O(5)-Co(1)-O(5) 90.7(3).

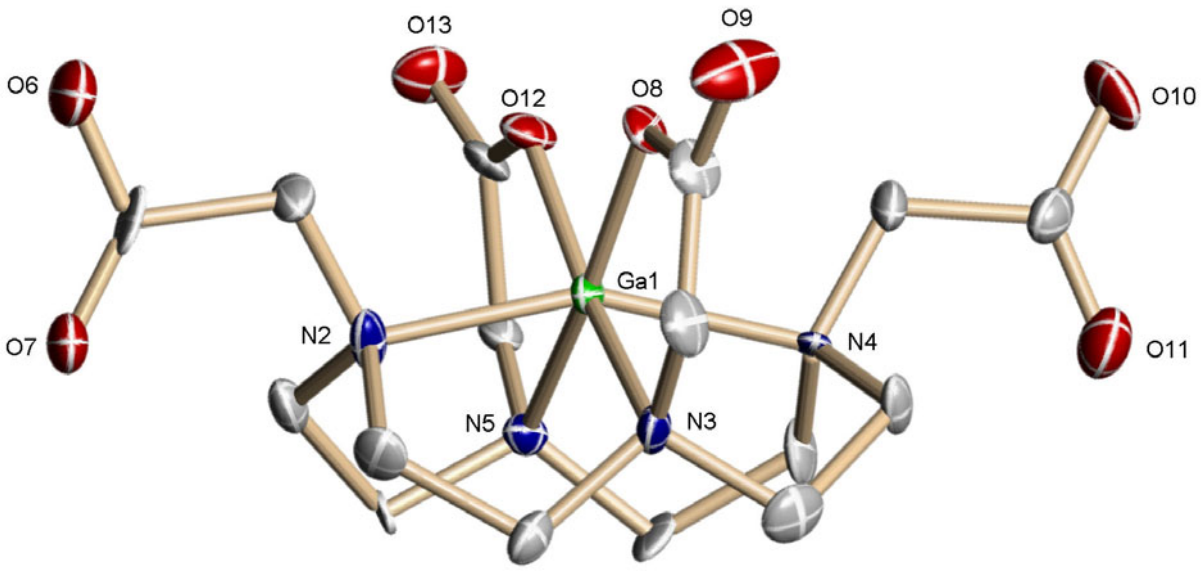

Figure 6. Ortep presentation of the X-ray structure $Ga^{III}(DOTA)^{-}$ (thermoparameter with 50% probability). Selected bond lengths [Å] and angles [°]: Ga(1)-N(3) 2.105(9), Ga(1)-N(5) 2.116(9), Ga(1)-N(2) 2.116(10), Ga(1)-N(4) 2.187(10), Ga(1)-O(8) 1.940(7), Ga(1)-O(12) 1.913(8); N(3)-Ga(1)-N(5) 109.0(2), O(12)-Ga(1)-O(8) 82.39(13), N(2)-Ga(1)-N(4) 157.1(2).

Improved pharmacokinetics and tumour targeting

Axel Heppeler, João P. André, Ingeborg Buschmann, Xuejuan Wang, Jean-Claude Reubi, Michael Hennig, Thomas A. Kaden, Helmut R. Maecke

Metal Ion-Dependent Biological Properties of a Chelator Derivatised Somatostatin Analogue for Tumour Targeting

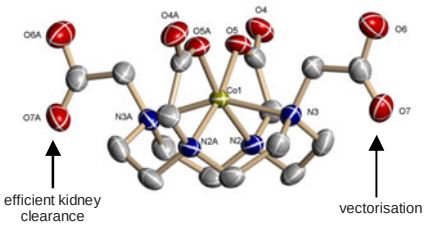

Improved pharmacokinetics and tumour targeting of a DOTA-conjugated somatostatin analogue was achieved by its coupling to the positron emitter ^{55}Co (^{57}Co). The structural features of the (radio)metal complex determine in vivo properties.